

Article

Damage Mechanism Analysis of the Connecting Screw of Turbine Disk-Drum Assembly

Haijun Wang ¹, Shengxu Wang ², Pu Xue ¹, Yongxin Guo ² and Liang Jiang ^{2,*} 

¹ School of Aeronautics, Northwestern Polytechnical University, 127 Friendship West Road, Xi'an 710072, China; 2020160669@mail.nwpu.edu.cn (H.W.); p.xue@nwpu.edu.cn (P.X.)

² College of Automation, Wuxi University, 333, Xishan Road, Wuxi 214105, China; wshx@cwuxu.edu.cn (S.W.); guoyx@cwuxu.edu.cn (Y.G.)

* Correspondence: jiangliangthu@tsinghua.org.cn

Abstract: The turbine disk-drum is one of the key components of an aero-engine and its assembly is connected with high-strength refined screws. But due to the uncoordinated rotation and deformation, the screws have abnormal wear damage. Through detailed contact stress analysis of screw body and component level using the finite element method, combined with experimental observation, the mechanism of wear damage of screw surface in screws is determined. It mainly includes the following: Firstly, the finite element method is used to calculate the deformation and stress distribution of the connecting screw of the turbine disk-drum assembly. Then, after the overspeed test, the morphology of the screws disassembled from the disk-drum assembly is evaluated. It was found that the wear degree in the circumferential direction and axial direction of the screw was quite different, that is, the screw wear experiment was consistent with the finite element analysis results. Finally, the influence of different rotation states and screw tightening states on screw wear was compared and analyzed. Conclusions obtained in this paper will be helpful to improve the assembly reliability of turbine drum.

Keywords: connecting screw; damage mechanism; finite element method; overspeed test



Citation: Wang, H.; Wang, S.; Xue, P.; Guo, Y.; Jiang, L. Damage Mechanism Analysis of the Connecting Screw of Turbine Disk-Drum Assembly. *Machines* **2024**, *12*, 489. <https://doi.org/10.3390/machines12070489>

Academic Editor: Ahmed Abu-Siada

Received: 12 June 2024

Revised: 17 July 2024

Accepted: 18 July 2024

Published: 19 July 2024



Copyright: © 2024 by the authors. Licensee MDPI, Basel, Switzerland. This article is an open access article distributed under the terms and conditions of the Creative Commons Attribution (CC BY) license (<https://creativecommons.org/licenses/by/4.0/>).

1. Introduction

Most of the high-pressure turbine components in aero-engines are composed of disk-drums. As an important part of the engine, they consist of high-pressure turbine disks, drum shafts, and labyrinth teeth disks, which are fixedly connected by screws at the rabbet. Due to the demanding working environment of high speed and high axial force, as well as the uneven distribution of screws preload, component manufacturing errors and assembly error, issues such as excessive screw contact stress and bending deformation can arise. These problems can further lead to screw bending deformation, surface thread damage, cracks, and even fractures [1]. This issue directly impacts the working performance of the turbine disk-drum assembly, increases the engine maintenance costs, poses safety risks, and affects the safety and reliability of the aero-engine [2]. There are many factors affecting the deformation and wear of the screws. The influencing mechanism is intricate, and the wear area and wear degree of the screw are unknown. It is necessary to consider the different factors affecting the wear of the connecting screws, investigate the deformation and wear mechanism, and predict the deformation results and wear degree and validate them.

In the study of the disc-drum assembly, Zou [3] investigated the disc rotor of the high-pressure compressor, the disc rotor of the high-pressure turbine, and the high-pressure rotor system. The finite element method and the experimental method were utilized to analyze the impact of changes in the mating surface preloading state on the dynamic characteristics of the rotor. Liu [4] established the dynamic model of the disc-drum rotor system with friction impact and analyzed its dynamic characteristics. Campos [5] presented a simplified method for determining the radial and circumferential stress of thin-walled cylindrical

structural parts with internal and external fits and also summarized the mechanical principles of the press-fit joint assembly, which can guide the analysis of the contact part of the rabbet. Liu [6] studied the stiffness characteristics of the flange joint at the rabbet based on the ANSYS nonlinear transient analysis method and plotted the hysteresis curve by applying harmonic load to extract displacement data. Additionally, Wang [7] simplified the screwed flange connection structure with a rabbet by using Jenkins unit and spring unit in parallel and analyzed the slip deformation mechanism of the rabbet between the contact interfaces. Panahi [8] presented an upgraded size-dependent formulation for micro-rotating shaft–disk systems to investigate their nonlinear forced vibration behavior. Su [9] utilized the Chebyshev polynomial as the admissible function to derive the motion equation of the rotating shell-plate combination and analyzed the influence of coupling stiffness and boundary conditions on the traveling wave frequency characteristics of the coupled structure for a single mode.

Many researchers use the finite element method to study contact stress and cracks. Hou [10] developed a rotor dynamics model considering screw flange connections using the finite element method and validated the results through ANSYS. Harish [11] also used the finite element method to investigate the factors influencing local contact stress and the initiation of cracks in screw connections. Ferjaoui [12] established a finite element model of screw connection structures and validated the life prediction model through experiments. Wang [13] described a computer-based finite element method for studying the stiffness and resistance behavior of beam–column moment joints in portal frames constructed by cold-formed steel back-to-back channel sections.

In the field of wear research, Liu [14,15] investigated the fretting wear of thread surfaces under longitudinal vibration by means of scanning electron microscopy and finite element simulation. Benhamena [16] studied the influence of contact stress on the fretting fatigue life of stud connection structures through experiments and finite element analysis, and developed a material response diagram. The findings indicate that the fretting fatigue life of the connection structure can be extended by increasing the contact stress within a certain range. Pedrosa [17] evaluated the short-term mechanical properties of an epoxy resin (steel reinforced resin) doped with steel bullets to consider its use in screw shear joints. Li [18] built two sets of mechanical properties test systems to test the dynamic parameters of the tangential and bending directions of the screw flange joint interface, and studied the mechanical behavior and dynamic parameters under different external excitations, screw distribution, and tightening torque. Zhou [19] and Zhang [20–22] revealed that fretting wear leads to changes in the distribution and magnitude of contact stress, which in turn affects the distribution of wear depth. The influence of bolt loosening on rotor dynamics was studied [23]. The motion equations for the rotor with bolt loosening are deduced, accounting for the local stiffness variation caused by the bolt loosening. Wu [24] studied High-Speed Rotor Vibration Failure Due to Sudden Angular Deformation of Bolt Joints. Analysis of the bolt joints in the faulty rotor reveals various phenomena such as joint interface damage, changes in bolt loosening torque distribution, and alterations in rotor initial unbalance.

In this paper, the finite element method is used to simulate and calculate the deformation of the connection part of the turbine disc drum assembly, considering various factors. The possible surface damage of the screw is analyzed through contact stress and contact interval. The main factors affecting the deformation and wear of the screw, as well as their degree of influence, are analyzed. The damage mechanism of the connecting stud of the disc drum assembly is studied, and the simulation results are validated through experiments.

2. Structure and Conditions

2.1. Basic Structure and Working Conditions

Structural composition: the turbine disk-drum assembly is composed of a high-pressure turbine disk (number 1 in Figure 1), a drum shaft (number 2 in Figure 1), and a labyrinth teeth disk (number 3 in Figure 1). This component is a simulated test piece based

on a high-pressure turbine disk of an aero-engine, and the high-pressure part is simulated and verified.

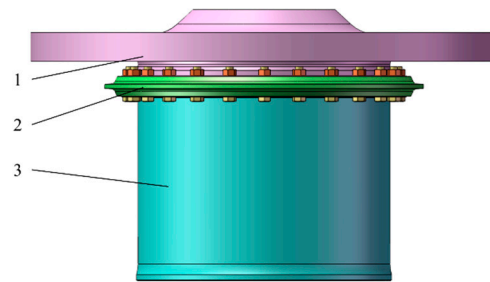


Figure 1. Turbine disk-drum assembly.

Structural state: the experimental simulation in this paper is assembled by 24 groups of circumferentially distributed screw components, and the connection part is at the rabbet. The screw is M10, the standard number is GB/T5780-2000 [25] and the performance level is 8.8. The cross-sectional view of the connection is shown in Figure 2.

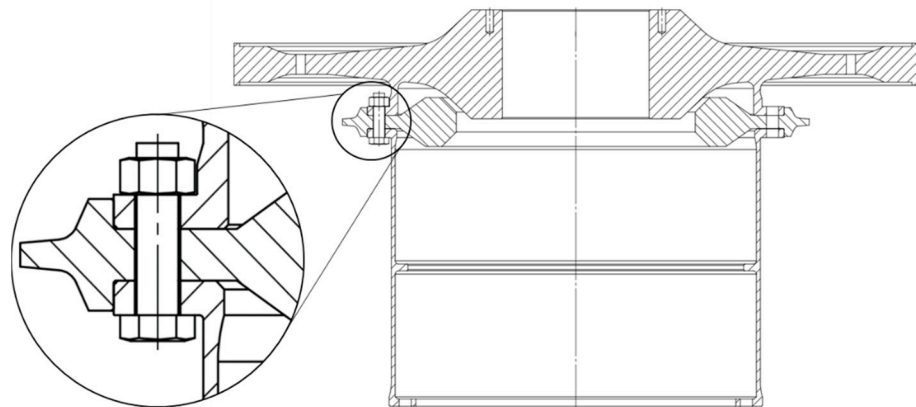


Figure 2. Section view of turbine disk-drum assembly.

Structural characteristics: firstly, numerous screws utilized to secure the drum shaft and the labyrinth teeth disk. However, due to the preload errors, some screws bear excessive force. Secondly, there is a significant diameter disparity between the high-pressure turbine disc and the drum shaft, with the high-pressure turbine disc being heavy. Under the working conditions of high speed, the centrifugal force generated by the high-pressure turbine disc is larger, and the connecting part is easy to deform for the thin-walled structure. This deformation leads to issues such as screw bending and damage to the contact surface.

Working state: As a part of the aero-engine rotor, the turbine disk-drum assembly can reach 18,000 rpm at work, and the overall temperature is approximately 600 °C under the action of high-temperature gas in the combustion chamber.

Boundary condition analysis:

(1) **Force:** As shown in Figure 3, under the action of high speed, the whole disk-drum assembly is subjected to a large centrifugal force F_1 . Under the action of high-temperature and high-pressure gas in the combustion chamber, the high-pressure turbine disk of the assembly is subjected to a large axial load, and the axial force F_2 can reach 200 kN. In order to ensure that the components remain tight, the screw connection must be given a certain pre-tightening force F_3 , which is set to 28 kN in this paper according to the assembly requirements of this type of aero-engine on site.

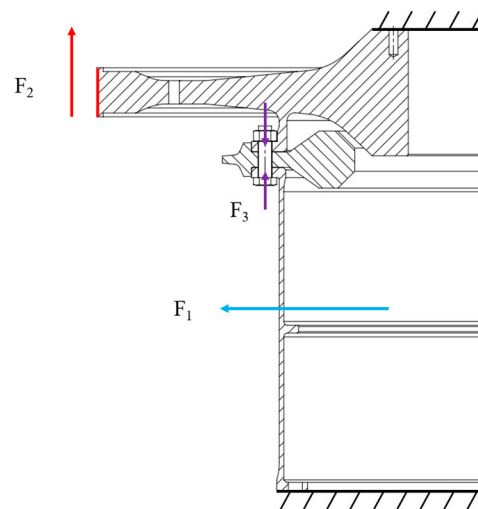


Figure 3. The force condition of disk-drum assembly.

(2) Constraints: The high-pressure turbine disk and the drum shaft of the turbine disk-drum assembly are tightly connected with the shaft through screws, so the upper surface of the high-pressure turbine disk and the lower surface of the drum shaft are fixed constraints. The force condition of the component is shown in Figure 3.

2.2. Analysis of Injury and Factors

In practical engineering, it is difficult to avoid the damage of parts and components after a long time of work. The deformation of parts size change and shape distortion due to excessive force. Because of the effect of contact stress, the surface material forms pitting or peeling surface fatigue wear. Small scars or gaps on the surface can occur under load.

Under the combined action of high speed and high axial force, the working conditions of the connecting part of the disc drum assembly are complex, and the factors affecting the deformation and surface wear of the screw are difficult to analyze. First of all, the deformation of the assembly makes screws and the inner surface of hole contact or even interfere, resulting in contact stress and contact area on the surface of the screw. Secondly, the contact stress and the contact area are related to the surface wear, which affects the screws state and may lead to early failure. Furthermore, contact and deformation may lead to excessive equivalent stress, causing fatigue failure of screws, resulting in cracks. Finally, the contact degrees of these contact surface are uncertain, and the contact between the nut and the connected part is also difficult to predict, and the stress distribution of the screw surface along the axis needs to be calculated and analyzed.

The direct cause of the screw damage are the deformation of the disc-drum assembly and the pulsation of the joint surface. Additionally, factors such as centrifugal force, preload force, preload force distribution, and others cannot be ignored. Therefore, this paper examines the impact of speed, preload, preload error, contact surface processing error, as well as the distribution and size of contact stress and equivalent stress on the screw under various conditions. It is essential to calculate the deformation and surface wear of the screw for further analysis.

2.3. Finite Element Modeling

2.3.1. Material Setting

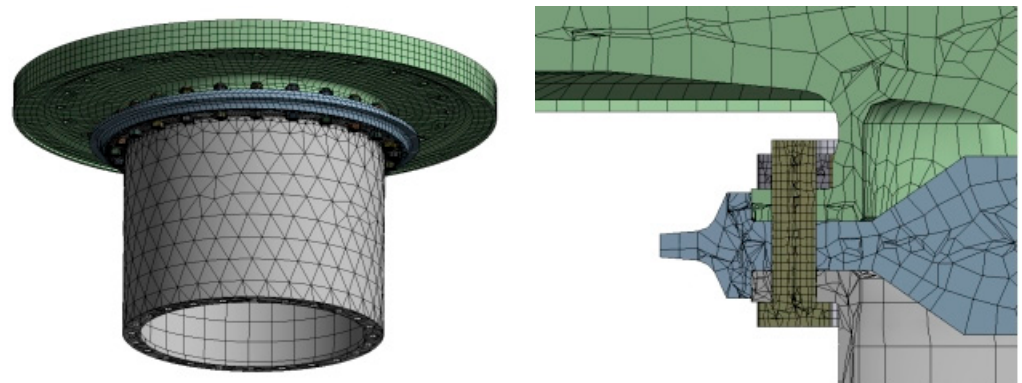
The main component material of the turbine drum assembly is nickel-based superalloy (GH4169). Poisson's ratio is 0.33 at operating temperature. The material setting is shown in Table 1. Connector materials such as screws are also GH4169. GH4169 has good comprehensive mechanical properties within a certain temperature range, and its comprehensive mechanical properties can be maintained at a relatively good level when it does not exceed 650 °C.

Table 1. GH4169 material setting (T = 600 °C).

| | Value | Unit |
|-------------------------------|-----------------------|-------------------|
| Density | 8240 | kg/m ³ |
| Young's modulus | 199 | GPa |
| Poisson's ratio | 0.33 | / |
| Thermal expansion coefficient | 1.48×10^{-5} | C ⁻¹ |
| Thermal conductivity | 21.2 | W/m·c |
| Ultimate tensile strength | 1000 | MPa |
| Yield strength | 860 | MPa |

2.3.2. Grid Meshing

The main part of the connection is the rabbet of the three parts, that is, the contact part of the screws and the joint surface of the three components are the key areas. When meshing, the connection part of the screw and the joint surface of the assembly are refined, and the disk surface of the high-pressure turbine disk and the drum shaft are simplified. After dividing the grid, there are 170,093 units and 557,309 nodes, as shown in Figure 4.

**Figure 4.** Grid division results.

The representation of the screw connection in simulation cannot be identical to the actual part due to interference issues. In the simulation, a simplified screw is considered to replace the standard screw model to calculate the displacement and stress. According to the research results of finite element analysis based on different modeling techniques in ANSYS Workbench screw connection, the solid elements without threads were employed to simplify the screw, neglecting thread contact.

2.3.3. Contact Setting

Frictional contact is set between the joint surfaces of high-pressure turbine disk, labyrinth teeth disk and drum shaft. According to the screw grade (8.8), 49 Nm is recommended as the tightening torque load. The statistical analysis of the preload force, the friction coefficient of the screw end face and the friction coefficient of the tooth surface under the tightening torque of each screw are shown in Table 2. The friction coefficient in the table is almost greater than 0.15, so the friction coefficient is set to 0.15.

Table 2. Friction coefficient of screw end face and tooth surface.

| Screw Number | Preload Force/N | Friction Coefficient of the Screw End Face | Friction Coefficient of the Tooth Surface |
|--------------|-----------------|--|---|
| 1 | 19,406.48 | 0.187 | 0.155 |
| 2 | 18,709.49 | 0.155 | 0.242 |
| 3 | 20,705.92 | 0.170 | 0.171 |
| 4 | 22,589.46 | 0.148 | 0.192 |
| 5 | 16,879.53 | 0.214 | 0.222 |

The three parts are tightly connected by screws, creating a 'Bonded' contact between the screw and the drum shaft. The screw and the labyrinth teeth disk, the nut and the disc surface of the high-pressure turbine, also have the same type of contact. There is no contact force between the screw and the hole, resulting in a 'Frictionless' contact between the screw and the screw hole of the three components. The contact settings are illustrated in Figure 5.

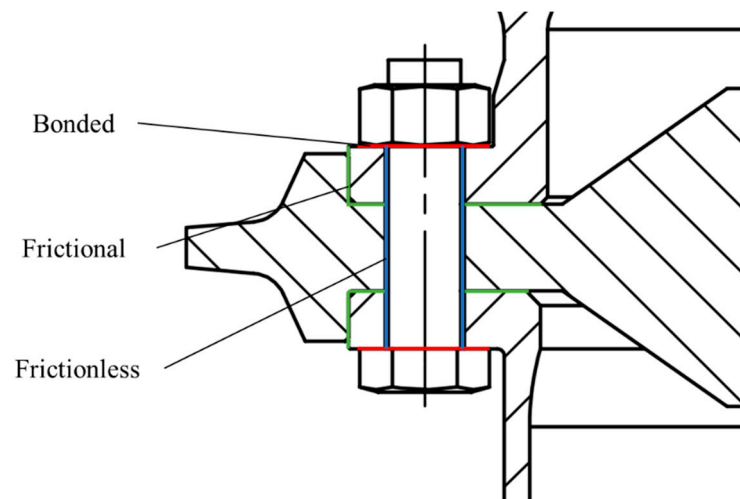


Figure 5. Contact settings.

2.3.4. Load and Constraint Setting

It can be seen from Section 2.1 that the disk-drum assembly is subjected to axial force, preload, centrifugal force, ambient temperature, and other factors. Referring to the actual aero-engine structure and working principle, a 200 kN axial force is applied to the outer surface of the high-pressure turbine disk, directed from the drum shaft to the high-pressure turbine disk along the axis. A pre-tightening force of 28 kN was applied to 24 groups of screws, with the action surface at the thread surface. A constant rotational speed of 18,000 rpm is applied to the entire drum assembly, and the ambient temperature is set to 600 °C.

In the entire rotor assembly, the bottom of the drum shaft is connected to the remaining components of the rotor, and the upper surface of the high-pressure turbine disk is fixedly connected to the conical cylinder by thread. This analysis assumes that the remaining components do not deform, thus the bottom of the drum shaft and the upper surface of the high-pressure turbine disk with threaded holes are set as fixed constraints. The load and constraint settings of the structure are shown in Figure 6.

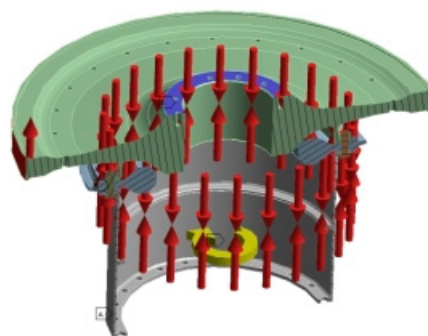


Figure 6. Load and constraint setting.

3. Analysis of Deformation and Stress of Screw under Different Rotational Speed

In this section, the deformation near the rabbet at different speeds is obtained by simulation, and the contact characteristics between the screw and the assembly are studied

from the deformation and stress distribution of the screw at different speeds. The speeds are set at 8000 rpm, 12,000 rpm, and 18,000 rpm, with the preload set equally at 28 kN.

3.1. Screw Deformation and Contact Conditions

Under the default speed of 18,000 rpm and the default preload of 28 kN, the deformation and stress distribution of the whole component and the screw are calculated, and some of the screw numbers are shown in Figure 7.

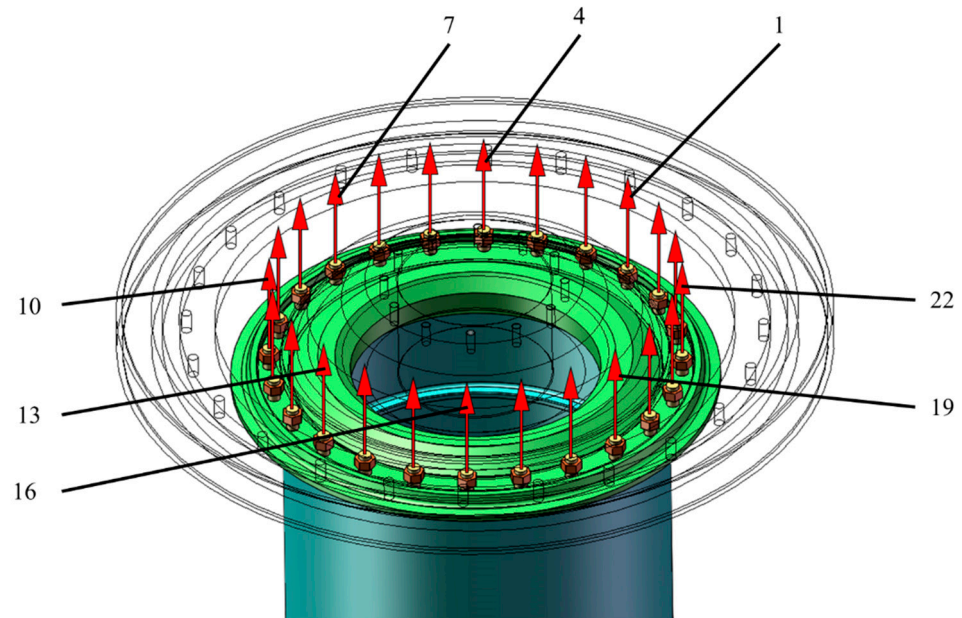


Figure 7. Screw distribution.

For the deformation, according to Figures 8–10, it can be seen that the deformations of the rabbet parts (drum shaft and labyrinth teeth disk) are not coordinated under the action of high speed. It means that positions of the connecting hole of the drum shaft (part 2 in Figure 1) and the labyrinth teeth disk (part 3 in Figure 1) are deformed, and the degree of deformation of the two is not the same. This phenomenon further leads to the bending deformation of the head and tail of the screw. The drum shaft has a large interference with the head end of the screw, while the interference between the high-pressure turbine disc and the tail end of the screw is small.

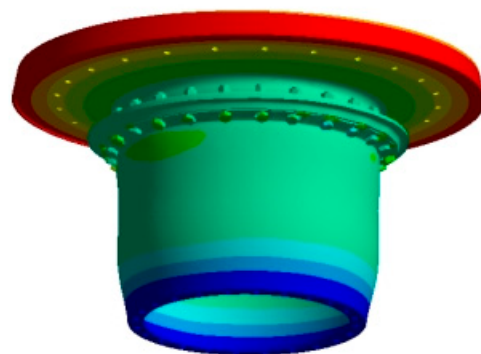


Figure 8. Overall component deformation.

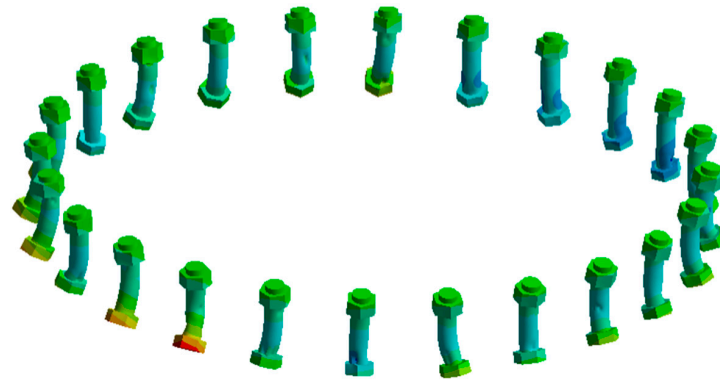


Figure 9. Deformation cloud picture.

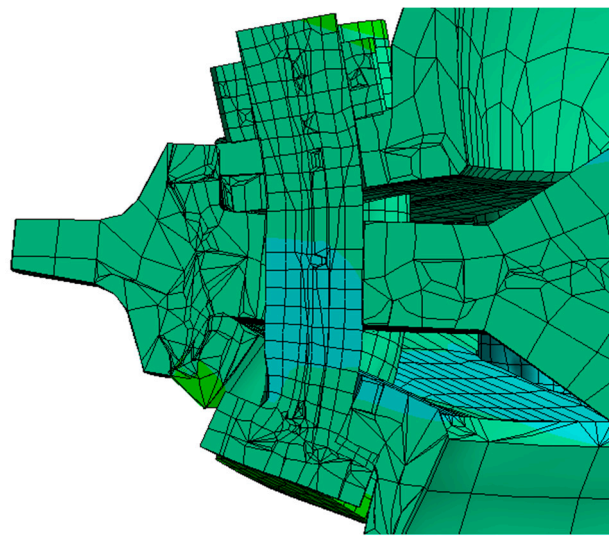


Figure 10. Equivalent stress cloud picture.

First of all, according to the contact stress distribution of the thread surface shown in Figure 11, it is evident that the deformation of the drum shaft has a large deformation and contact stress on the head end of the screw due to the uncoordinated deformation. Secondly, the axis side of the disc drum assembly of the screw surface is defined as the inner side of the screw ring. Figure 12 indicates that the stress within the screw ring is generally higher than the stress outside the screw ring. Finally, based on the analysis in Figure 8, the reason for the higher stress on the inner side of the screw ring is that the drum shaft only squeezes the inner side, while the larger opening and closing phenomenon occurs on the outer side of the screw ring.

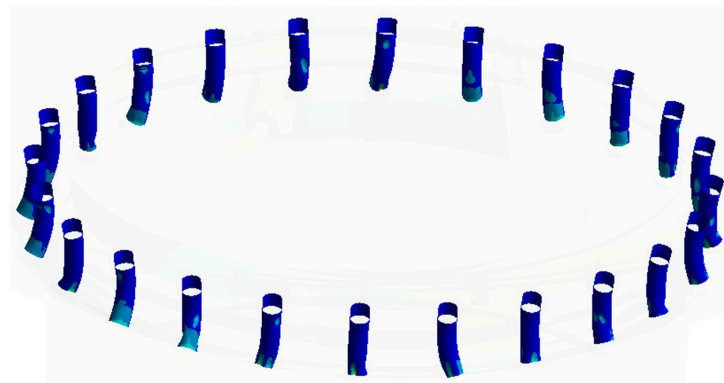


Figure 11. Contact stress distribution.

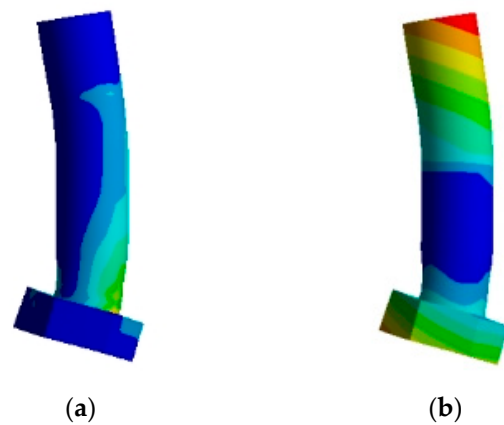


Figure 12. Stress (a) and deformation (b) cloud picture of screw No.1.

3.2. Comparative Analysis

The screw deformation at different speeds is shown in Figure 13, illustrating the deformation state under a 25 times displacement field. When compared to the speed of 18,000 rpm, bending deformation still occurs at low speeds due to uncoordinated deformation. However, at lower speeds, the bending degree decreases, resulting in a reduction in the contact force of the screw.

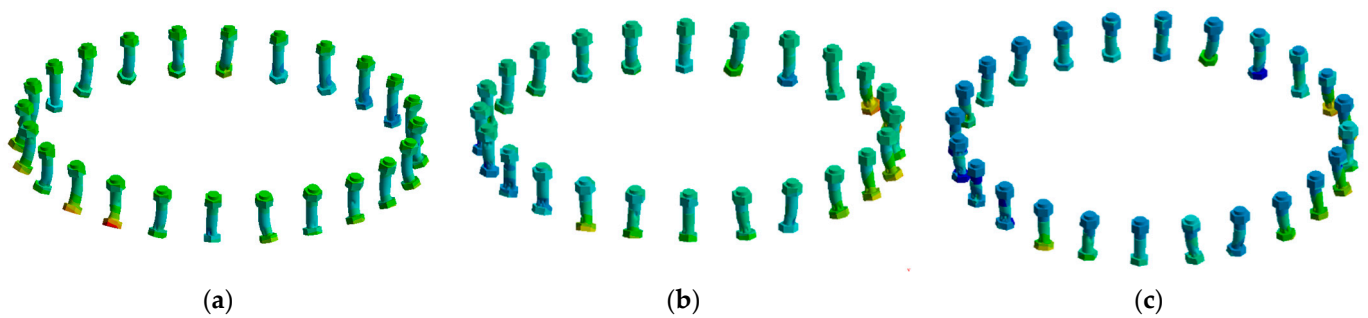


Figure 13. Deformation cloud picture at different speeds. (a) 18,000 rpm; (b) 12,000 rpm; (c) 8000 rpm.

For stress situations. Based on the analysis of Figure 14, it can be seen that as the rotation speed decreases, the area with higher stress inside the screw ring is significantly reduced, leading to a decrease in equivalent stress. When the speed drops to 8000 rpm, there is almost no difference in stress between the inner and outer sides of the screw ring. However, the position with higher stress remains concentrated at the head end of the screw rather than the tail end.

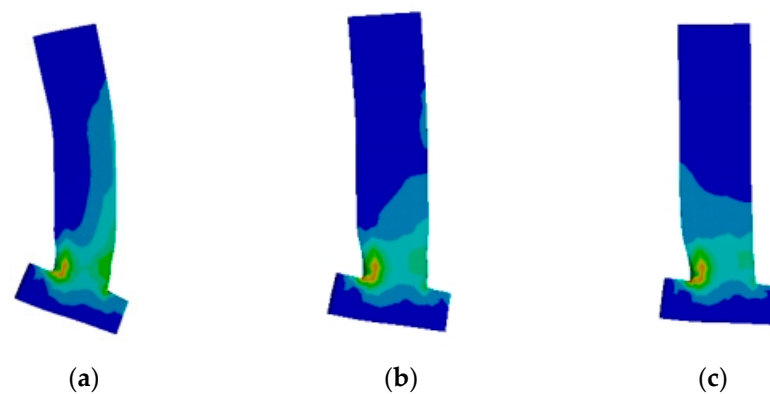


Figure 14. The equivalent stress cloud picture of the screw section at different rotational speeds. (a) 18,000 rpm; (b) 12,000 rpm; (c) 8000 rpm.

The incongruity arises from the deformation of the rabbit. Although the level of incompatibility gradually diminishes as the rotational speed decreases as shown in Figure 15, it still exerts pressure on the head and tail ends of the screw and causes deformation. Simultaneously, the interference between the screw's head end and the drum shaft is more serious than that at the tail end. This is primarily because the tail end of the screw can slide relative to the high-pressure turbine disk, and the drum shaft can only generate significant extrusion force with the screw under the blocking effect of the screw head.

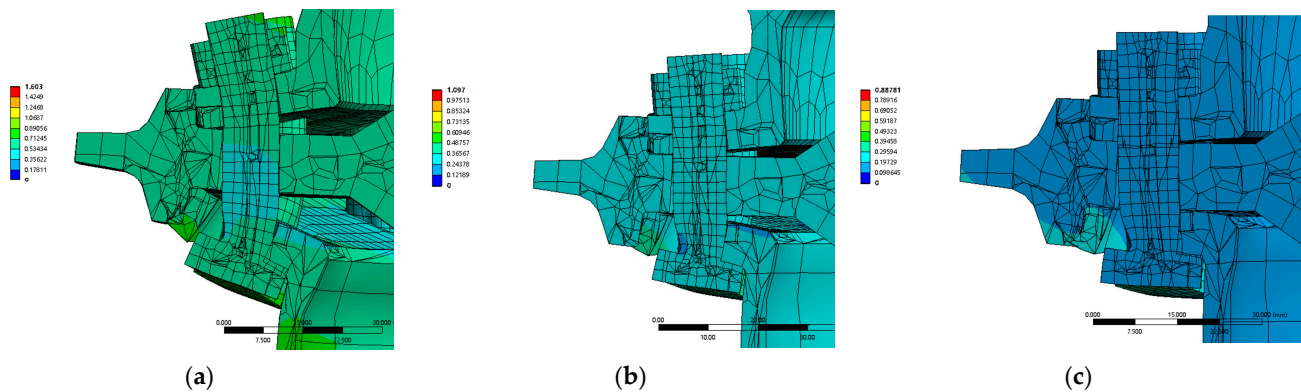


Figure 15. Nozzle deformation at different speeds. (a) 18,000 rpm; (b) 12,000 rpm; (c) 8000 rpm.

3.3. Result and Discussion

At low speeds, stress concentration primarily occurs at the head of the screw and is evenly distributed in the circumferential direction. In contrast, the stress at the tail of the screw is small. Consequently, the wear parts are concentrated at the head of the screw, and the wear of the screw surface is inconsistent in the circumferential distribution.

At high speeds, due to the uncoordinated deformation of the components, the extrusion pressure of the drum shaft on the screw increases. The main contact area is on the inner side of the screw ring at the head end. Consequently, the inner side of the screw ring is more susceptible to surface wear and even cracks. This indicates that the wear of the screw in different positions in the circumferential direction of the screw will be different.

The stress at the head end of the screw is typically higher than that at the tail end. This is because of the interference between the screw's head end and the drum shaft, causing deformation, while relative sliding can occur between the tail end of the screw and the high-pressure turbine disk. Therefore, the tail end of the screw is more prone to surface wear.

4. Analysis of the Influence of Different Preload Distribution on Screw Wear

The connection of the disc-drum combined mechanism is primarily secured by 24 sets of circumferential screws in a series. When the pre-tightening force is unevenly distributed, it is easy to cause local stress concentration of the screws and even serious damage. In this section, the impact of varying preload distribution on the deformation and stress distribution of the screws under high speed, and analyzes how uneven preload affects the damage to the screws.

4.1. Different Preload Settings

In the actual assembly process, due to the influence of surface processing errors, friction coefficient, and other factors, it is difficult to ensure the consistency of preload. Simultaneously, at high rotation speeds, the stress distribution of the screw tends to be uneven, leading to wear site concentration. Therefore, considering the pre-tightening force distribution type under the condition of 18,000 rpm speed, the default pre-tightening force of 28 kN is taken as the standard value, the maximum pre-tightening force is 32 kN, and the minimum pre-tightening force is 24 kN. The pre-tightening force distribution type is

divided into three types: double-peak double-high, double-peak single-high, and single-peak single-high, and are defined as states 1, 2, and 3, respectively. The equal pre-tightening force distribution is defined as state 4. The pre-tightening force distribution is illustrated in Figure 16.

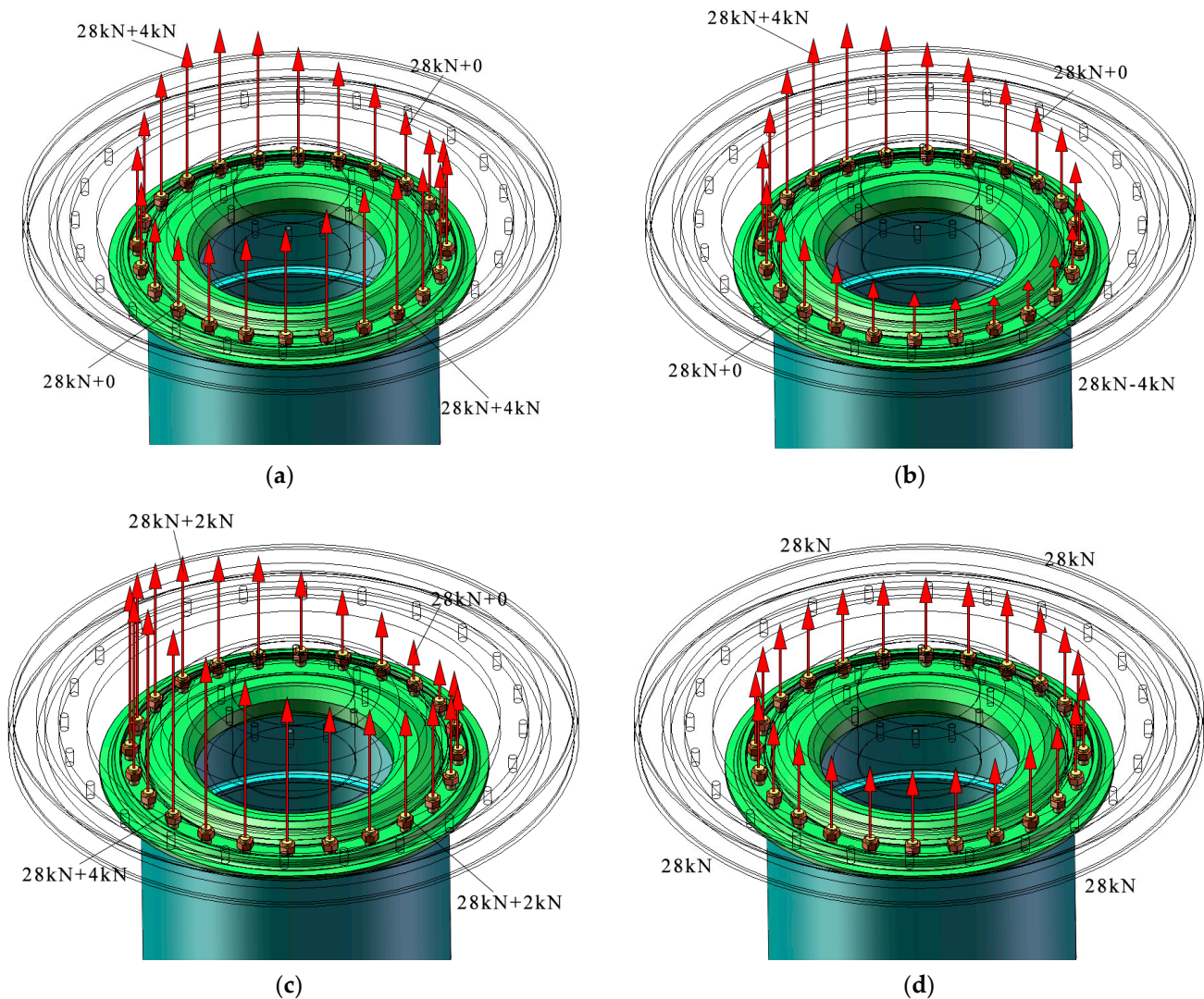


Figure 16. Preload distribution type. (a): Double-peak and double-high pre-tightening force distribution; (b): double-peak single-high preload distribution; (c): single-peak single-high pre-tightening force distribution; (d): uniform pre-tightening force distribution.

Due to the large number of screws, the screws in special positions are selected for deformation analysis. Considering the three distribution conditions, No.1, 7, 13 and 19 are taken to analyze the deformation of the three distribution conditions. They are marked in Figure 7, and the preload is set as shown in Table 3.

Table 3. Pre-tightening force of selected screws.

| No. | Pre-Tightening Force/kN | | | |
|-----|-------------------------|---------|---------|---------|
| | State 1 | State 2 | State 3 | State 4 |
| 1 | 28 | 28 | 28 | 28 |
| 7 | 32 | 32 | 30.828 | 28 |
| 13 | 28 | 28 | 32 | 28 |
| 19 | 32 | 24 | 30.828 | 28 |

4.2. Distribution of Stress

According to the finite element analysis, the stress distribution of the screw under different preload conditions is calculated. The deformation of the screw under four distribution types is shown in Figure 17.

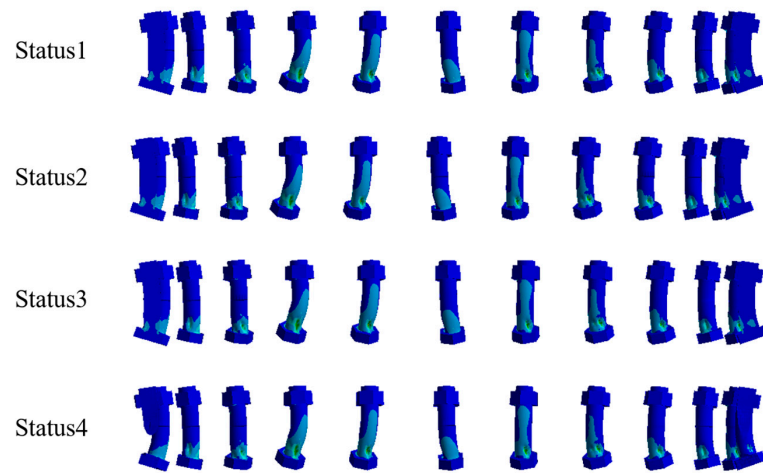






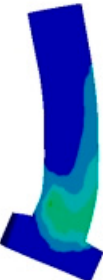



Figure 17. Stress distribution.

The stress distribution and deformation of No.1, 7, 13 and 19 screw sections under four distribution types are shown in Table 4. In the case of different pre-tightening force distribution, the difference of stress distribution is small, and the position with higher stress remains in the inner part of the screw ring, indicating that the pre-tightening force distribution has little effect on the position distribution of the screw crack. Moreover, the pre-tightening force distribution also has little effect on the deformation. Under the condition of equal pre-tightening force, the stress distribution and maximum stress of different screws are vary significantly, which should be taken into account when comparing the maximum stress of different pre-tightening force distributions.

Table 4. Stress distribution of single screw.

| No. | Double-Peak Double-High | Double-Peak Single-High | Single-Peak Single-High | Equal Pre-Tightening Force Distribution |
|-----|-------------------------|-------------------------|-------------------------|---|
| 1 | | | | |
| 7 | | | | |

Table 4. Cont.

| No. | Double-Peak Double-High | Double-Peak Single-High | Single-Peak Single-High | Equal Pre-Tightening Force Distribution |
|-----|---|---|---|---|
| 13 |  |  |  |  |
| 19 |  |  |  |  |

4.3. Maximum Stress Condition

It can be seen from Section 4.2 that although the preload is the same, the stress distribution and the maximum stress may still be different, so the maximum stress difference Δ is taken by Equation (1).

$$\Delta = \sigma'_{\max} - \sigma_{\max} \quad (1)$$

σ'_{\max} —The maximum stress of a single screw under non-uniform preload distribution.

σ_{\max} —The maximum stress of a single screw with uniform preload distribution.

The maximum stress and pre-tightening force of the screw are shown in Figure 18. The diagram indicates that as the preload increases, the maximum stress of the screw increases, on the contrary, it decreases. In the case of double-peak and double-high preload distribution, the maximum stress of the screws at different positions is quite different, and the maximum stress of the No.19 screw is larger. The larger the pre-tightening force error range, the greater stress change in different screws is not necessarily caused. The distribution of pre-tightening force is more likely to cause inconsistent maximum stress and potentially lead to higher stress levels.

4.4. Result and Discussion

The distribution of different preloads has minimal impact on the deformation and stress distribution of the screw. The main wear parts are still located within the screw ring, and cracks are more likely to develop at the head end.

Compared to the magnitude of the pre-tightening force, the distribution of the pre-tightening force has a more significant impact on the crack. In the assembly process, it is necessary to ensure that the pre-tightening force is consistent as far as possible, so as to avoid the problems of high unilateral pre-tightening force or fluctuations in pre-tightening force.

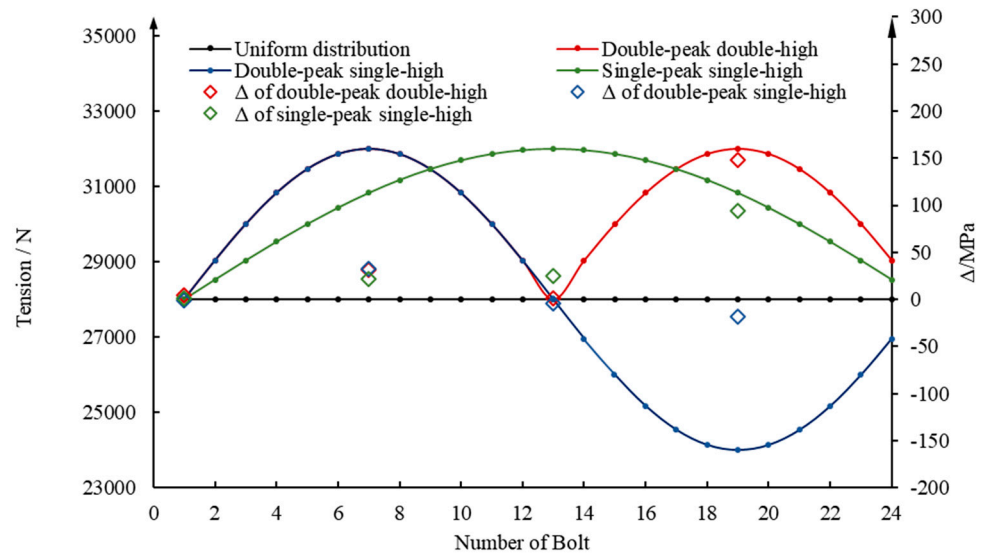


Figure 18. Pre-tightening force and maximum stress.

5. Qualitative Observation of the Experiment

Taking the disc-drum connection component as the experimental object, different speeds were applied by the rotating test bench. Long-term operation was carried out to produce wear to obtain the damaged parts. The morphology and distribution of the wear on the screw surface were analyzed, and the simulation results were compared to validate the above analysis.

5.1. Experimental Platform and Test System

The experimental platform utilizes a self-built vertical rotating experimental platform. The disc-drum connector is installed on the platform through the fixture, and the actual speed of the disc-drum connector is converted by the speed increaser. The structure of the experimental platform is shown in Figure 19 (the total height is approximately 3.6 m). The Siemens LMS test system is used to collect the rotating eddy current signal and the vibration acceleration signal. The real-time signal display in the time-frequency domain is configured by the accompanying software, aiding in monitoring the rotational stability of the component and conducting future overall vibration analysis.

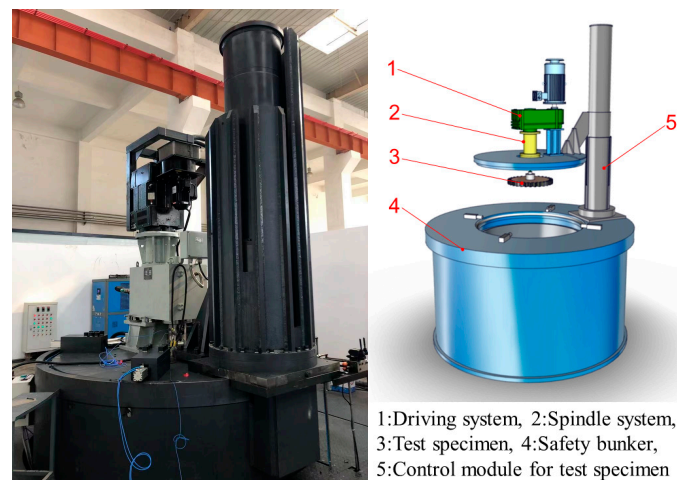


Figure 19. Schematic picture of the overspeed test bench.

5.2. Experimental Design and Experimental Methods

Firstly, speed-up and speed-down experiments were conducted to determine the critical first-order speed. Secondly, avoiding the critical speed, the influence of different working conditions on the surface wear of the screw was studied when the stable speed was running. Finally, the wear of the screw surface was observed and analyzed, and the regular conclusion was given.

Three rotational speeds of 1200 rpm, 2400 rpm and 3600 rpm were applied to the experimental parts to simulate the effect of different rotational speeds on surface wear.

To simulate the pre-tightening force, the torque wrench was used to control the pre-tightening torque of screws (M10) in the circumferential direction, which is $M = 56 \text{ N}\cdot\text{m}$. It can be seen from Section 4.2 that the change in preload has little effect on the change in surface wear, so the magnitude and distribution of preload are not considered. On this basis, a 30 g screw was applied to the turbine disk directly above the No.1 screw to simulate the unbalance, as shown in Figure 20.

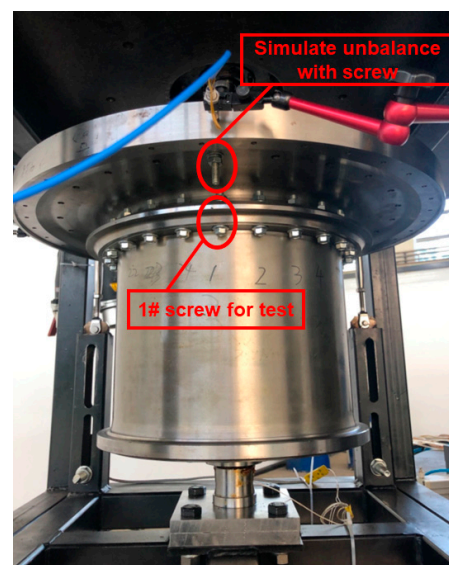


Figure 20. Test condition setting: unbalanced mass.

According to the working conditions described above, the disk-drum connection component was installed, and the test bench was initiated. Once the speed stabilized, timing commenced, and data were measured and recorded. Data collection occurred every 10 min, and the machine was halted after 120 min of steady operation. Subsequently, all screws were removed to inspect the wear on the screw surface.

5.3. Experimental Result

After 120 min of stable operation at each speed, the screw wear parts were obtained. The threads showed wear under different working conditions, but the variances were minimal. This was attributed to the challenge of running for thousands of hours without significant deviations. Hence, this study focused on the screw wear at the lowest speed.

Considering the effect of unbalanced mass, the thread area of the No.1 screw appears thicker by naked eye, indicating significant wear, as shown in Figure 21b. At this time, the screw cannot be disassembled with a torque of $56 \text{ N}\cdot\text{m}$ (the torque used during assembly), and the torque must be increased to $70 \text{ N}\cdot\text{m}$ that the screw can be disassembled. It means the preload is increased, indicating that the experiment obviously caused the surface wear of the screw.

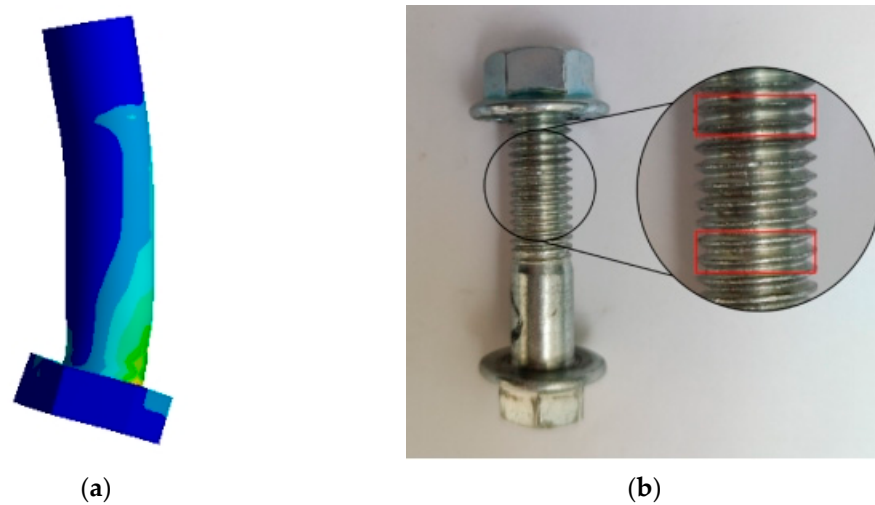


Figure 21. Comparison of wear results. (a) result of finite element calculation; (b) result of wear test.

According to the calculation results of the Section 3.1, the stress distribution in the axial and circumferential directions is inconsistent. The wear test piece in Figure 21b shows that the thread wear on the head side of the screw is significantly more severe than that on the tail end, which verifies that the stress on the head end of the screw is greater than that on the tail end.

The wear of the same screw at different positions in the circumferential direction of the screw surface is illustrated in Figure 22. It is evident that the wear at the head end of the screw in different circumferential directions is more severe than that at the tail end. At the same time, at the end of the screw, the wear at different positions in the circumferential direction is obviously different, which verifies the rationality of different circumferential stress distribution.

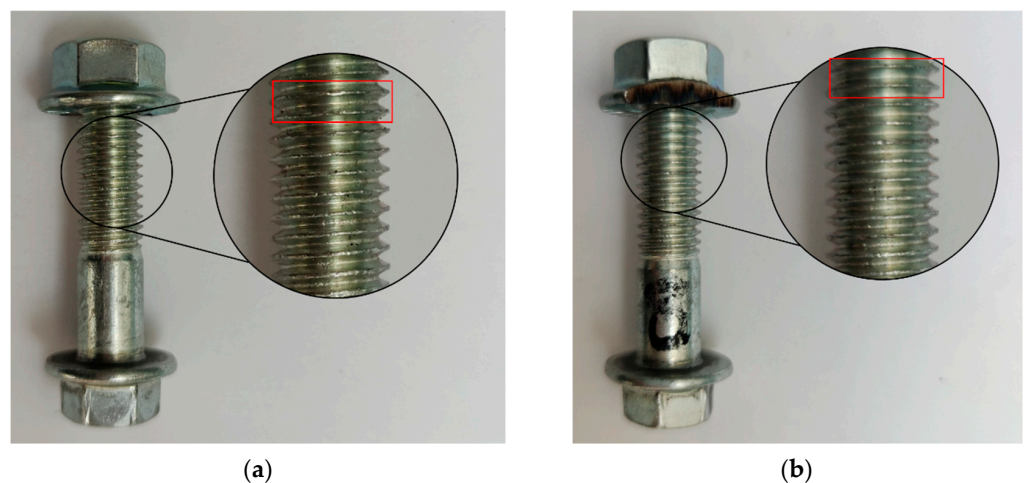


Figure 22. Circumferential wear comparison. (a) serious wear; (b) light wear.

6. Conclusions

The connecting screw of the turbine disk-drum assembly was taken as the research subject. The finite element method was utilized to compute the deformation and stress of the connecting screw considering the rotational speed and preload distribution. The causes of screw deformation and wear are explored. The main wear areas and conditions of the screw are analyzed, and the rationality of the calculation results is verified by experiments.

Firstly, the primary causes of deformation and stress concentration are analyzed. When the rotational speed is high, the connection point of the parts in the turbine disk-drum

assembly will produce serious deformation inconsistency. This phenomenon is particularly noticeable at 1800 rpm, with a deformation difference of up to 0.04 mm. Simultaneously, due to the deformation and extrusion of the parts, stress concentration and wear on the screw are caused. The analysis indicated that the uneven distribution of preload has minimal impact on the screw.

Then, according to the stress distribution analysis, the area most susceptible to severe wear was obtained. The head end of the screw, experiencing higher stress, is more prone to wear. The stress at the tail end of the bolt is only 22% of that at the head end. Furthermore, the wear of the screw surface is inconsistent in the circumferential distribution, and the majority of wear mainly concentrated on the axis side of the turbine disk-drum assembly. The side with higher stress is approximately 49% more stressed than the other side.

Finally, the wear experiment of the screw was conducted. The experimental results show that the wear distribution of the screw surface is consistent with the finite element calculation results, validating the rationality of using the finite element method to analyze the wear mechanism and wear condition of the screw.

The research conducted in this paper analyzes the mechanism of screw damage, which is helpful to analyze the cause of screw damage in turbine disk-drum assembly and predict the wear conditions.

Author Contributions: Conceptualization, H.W. and L.J. and P.X.; methodology, H.W. and S.W.; software, H.W.; validation, S.W., Y.G. and P.X.; formal analysis, H.W.; investigation, H.W.; resources, P.X.; data curation, S.W.; writing—original draft preparation, H.W.; writing—review and editing, S.W.; visualization, Y.G.; supervision, L.J.; project administration, L.J.; funding acquisition, P.X. All authors have read and agreed to the published version of the manuscript.

Funding: This research was funded by the National Natural Science Foundation of China, grant numbers 12072288 and 12272319.

Data Availability Statement: Data are contained within this article.

Conflicts of Interest: The authors declare no conflict of interest.

References

- Shigley, J.E.; Mischke, C.R. *Fastening, Joining, and Connecting: A Mechanical Designers' Workbook*; McGraw-Hill Publishing Company: New York, NY, USA, 1990.
- Iyer, K.; Hahn, G.T.; Bastias, P.C.; Rubin, C.A. Analysis of fretting conditions in pinned connections. *Wear* **1995**, *181–183*, 524–530. [[CrossRef](#)]
- Zou, C.; Xia, H.; Chen, K.; Zhai, J.; Han, Q. Research on the identification method of the pre-tightening state of the matching surface of the aero-engine disk-drum rotor. *Eng. Fail. Anal.* **2022**, *136*, 106208. [[CrossRef](#)]
- Liu, L.; Cao, D.; Sun, S. Dynamic characteristics of a disk–drum–shaft rotor system with rub-impact. *Nonlinear Dyn.* **2015**, *80*, 1017–1038. [[CrossRef](#)]
- Campos, U.A.; Hall, D.E. Simplified Lamé's equations to determine contact pressure and hoop stress in thin-walled press-fits. *Thin-Walled Struct.* **2019**, *138*, 199–207. [[CrossRef](#)]
- Liu, Y.; Wang, J.; Chen, L. Dynamic Characteristics of the Flange Joint with a Snap in Aero-Engine. *Int. J. Acoust. Vib.* **2018**, *23*, 168–174. [[CrossRef](#)]
- Wang, Z.; Li, K.; Liu, Y. Stiffness characteristics of flange joint with a snap and its influence on structure vibration. *J. Aerosp. Power* **2019**, *34*, 1201–1208. (In Chinese)
- Panahi, R.; Asghari, M.; Borjalilou, V. Nonlinear forced vibration analysis of micro-rotating shaft–disk systems through a formulation based on the nonlocal strain gradient theory. *Arch. Civ. Mech. Eng.* **2023**, *23*, 85. [[CrossRef](#)]
- Su, Z.; Jin, G.; Ye, T. Free vibration analysis of moderately thick functionally graded open shells with general boundary conditions. *Compos. Struct.* **2014**, *117*, 169–186. [[CrossRef](#)]
- Hou, X.; Luo, Z.; Huang, Y.; Zhang, X. Vibration characteristics analysis of rotor system with screw connection. *Aerospace* **2018**, *44*, 17–23. (In Chinese)
- Harish, G.; Farris, T. *An Integrated Approach for Prediction of Fretting Crack Nucleation in Riveted Lap Joints*; E. Flammarion: Paris, France, 2013.
- Ferjaoui, A.; Yue, T.; Wahab, M.A.; Hojjati-Talemi, R. Prediction of fretting fatigue crack initiation in double lap screwed joint using Continuum Damage Mechanics. *Int. J. Fatigue* **2015**, *73*, 66–76. [[CrossRef](#)]
- Wang, F.; Han, Y.; Yang, J. Nonlinear FE analysis on stiffness and resistance of screwed cold-formed steel built-up joints. *Structures* **2021**, *33*, 2520–2533. [[CrossRef](#)]

14. Liu, J.; Ouyang, H.; Peng, J. Experimental and numerical studies of screwed joints subjected to axial excitation. *Wear* **2016**, *346–347*, 66–77. [[CrossRef](#)]
15. Liu, J.; Ouyang, H.; Feng, Z.; Cai, Z.; Liu, X.; Zhu, M. Study on self-loosening of screwed joints excited by dynamic axial load. *Tribol. Int.* **2017**, *115*, 432–451. [[CrossRef](#)]
16. Benhamena, A.; Amrouche, A.; Talha, A.; Benseddiq, N. Effect of contact forces on fretting fatigue behavior of screwed plates: Numerical and experimental analysis. *Tribol. Int.* **2012**, *48*, 237–245. [[CrossRef](#)]
17. Pedrosa, B.; Buecking, L.; Veljkovic, M. Steel-reinforced resin for screwed shear connectors: Confined behaviour under quasi-static cyclic loading. *Eng. Struct.* **2022**, *256*, 114023. [[CrossRef](#)]
18. Li, T.; Yang, D.; Zhao, B.; Sun, Q.; Huo, J.; Sun, W. Measured and investigated nonlinear dynamics parameters on screwed flange joints of combined rotor. *J. Mech. Sci. Technol.* **2021**, *35*, 1841–1850. [[CrossRef](#)]
19. Zhou, J.; Liu, J.; Ouyang, H.; Cai, Z.; Peng, J.; Zhu, M. Anti-Loosening performance of coatings on fasteners subjected to dynamic shear load. *Friction* **2018**, *6*, 32–46. [[CrossRef](#)]
20. Zhang, M.; Zeng, D.; Wang, Z.; Tang, M.; Lu, L. Loosening Evaluation of screwed Joints Modified by Fine Particle Bombardment under Transverse Cyclic Loading. *Tribol. Trans.* **2018**, *61*, 1003–1012. [[CrossRef](#)]
21. Zhang, M.; Lu, L.; Wang, W.; Zeng, D. The roles of thread wear on self-loosening behavior of screwed joints under transverse cyclic loading. *Wear* **2018**, *394*, 30–39. [[CrossRef](#)]
22. Zhang, M.; Zeng, D.; Lu, L.; Zhang, Y.; Wang, J.; Xu, J. Finite element modelling and experimental validation of screw loosening due to thread wear under transverse cyclic loading. *Eng. Fail. Anal.* **2019**, *104*, 341–353. [[CrossRef](#)]
23. Qin, Z.; Han, Q.; Chu, F. Bolt loosening at rotating joint interface and its influence on rotor dynamics. *Eng. Fail. Anal.* **2016**, *59*, 456–466. [[CrossRef](#)]
24. Wu, F.; Hong, J.; Chen, X.; Ma, Y. Analysis of High-Speed Rotor Vibration Failure Due to Sudden Angular Deformation of Bolt Joints. *Symmetry* **2023**, *15*, 1937. [[CrossRef](#)]
25. GB/T5780-2000; Hexagon Head Bolts. Product Grade C. The Standardization Administration of the People’s Republic of China: Beijing, China, 2001.

Disclaimer/Publisher’s Note: The statements, opinions and data contained in all publications are solely those of the individual author(s) and contributor(s) and not of MDPI and/or the editor(s). MDPI and/or the editor(s) disclaim responsibility for any injury to people or property resulting from any ideas, methods, instructions or products referred to in the content.